The paper has been prepared for submission to **Sensors and Actuators A: Physical.**

Analysis of the multi-balloon dielectric elastomer actuator for traveling wave motion

Yujin Jang*, Hiroyuki Nabae, Gen Endo and Koichi Suzumori

Department of Mechanical Engineering, School of Engineering, Tokyo Institute of Technology, 2-12-1, Ookayama, Megro-ku, Tokyo 152-8550, Japan

* Correspondence: jang.y.aa@m.titech.ac.jp

Abstract

Recently, various soft actuators with biologically inspired motions have emerged in the field of robotics. The present study focuses on the development of a multi-balloon dielectric elastomer actuator (DEA) to provide a traveling wave motion for the linear transportation of an object. The multi-balloon actuator is designed on the basis of a pneumatic rubber actuator and a DEA, which itself consists of a dielectric membrane mounted on a silicone air chamber. An actuator that is inflated by pre-charged air pressure induces a rapid response speed and large deformations using only electric power; thus, it does not require the bulky external system which is essential for conventional pneumatic actuators. A multi-balloon actuator made of only soft materials was successfully fabricated by screen printing, rubber casting, and plasma treatment processes. Throughout the experiment, the maximum displacements of the balloon actuator with respect to height and width were obtained at an air pressure of 12.2 kPa. Importantly, the multi-balloon actuator's components assembled and interacted with each other and could successfully transport an object linearly via a traveling wave. In the object transfer experiment of this study, the linear velocity reached 0.97 mm/s with an initial air pressure and the applied voltage maintained at 13.3 kPa and 7.5 kV, respectively. The potential applicability of this system as a portable robot is demonstrated by replaying the traveling wave motions using a multi-balloon actuator. In the future, this design can be applied to portable small-scale robots and annelid robots with high reliability and body compliance.

Keywords: Dielectric Elastomer Actuator, Multi-balloon Actuator, Traveling wave Motion, Soft Robot, Pre-stretching

---

1. Introduction

Soft actuators, consisting of flexible materials such as rubbers, gels, or polymers, are attracting attention for their advantage over conventional rigid actuators owing to their flexible mechanisms which can move and change adaptively. A typical biomimetic motion employed by soft actuators is the traveling wave operation. It has been applied to a variety of soft actuators in different materials and configurations such as magnetostrictive inchworms [1], pneumatic snake robots [2], piezoceramics [3], annelid robots [4], and artificial muscles [5].

Among soft actuators, pneumatic rubber actuators have been introduced to produce large deformations and high forces [6]-[7]. For these reasons, various types of soft-bodied actuators that generate traveling or peristaltic wave motion have been reported. For example, the pneumatic rubber actuator, which consists of multiple air chambers, has been proposed to assist colonoscope insertion [8]. In addition, a planar-type pneumatic actuator using several rubber balls was developed for transportation in planar dimensions [9]. These pneumatic actuators can be driven periodically by controllable air pressure in each segment. However, pneumatic actuators additionally rely on bulky mechanical devices such as compressors, tanks, regulators, and gas sources. These external factors can limit the flexibility and practical applications when applied to portable systems. In addition, there are limitations on the actuating frequency owing to a slow response rate.

Alternatively, dielectric elastomer actuators (DEAs), a type of electroactive polymer actuator, have fast response times, high energy density, and quiet operation [10]. For these reasons, DEAs have been applied in various fields such as biomimetics [11], bending actuator using triangular dielectric elastomer minimum energy structure (DEMES) [12], and artificial muscles [13]. Typically, DEAs consist of a dielectric elastomer (DE) membrane coated on both sides with compliant electrodes. The strain of the elastomer membrane is induced by a Coulomb force when voltage is applied to the electrodes. However, the elastomer membrane should be pre-stretched to allow it to generate large deformations. Most DEAs are stretched using mechanical rigid elements [14]-[15], which limits the direction of motion and lowers the system's flexibility.

Another way to increase strain is to use pneumatics [16] or hydraulics [17] to create inflated structures. They have potential in various applications such as locomotive robot [18], multi-directional dome actuator for space [19], fluid pumps [20], soft tactile interfaces [21], and hemispherical speakers [22]. When air or water pressure is pre-applied to a membrane, the shape of DEA is deformed like balloon, and can perform out-of-plane motions, which can also result in complex non-linear deformations [23]. Typically, inflated DEAs are made from acrylic elastomers that can experience snap-through instability and therefore exhibit a good performance in terms of deformations when activated. An improvement in the area strain from 158% to 1,692% has been reported [24]-[26]. However, after triggering mass inflation, the amount of air in the chamber needs to be changed to implement a reversible and repeatable motion. In addition, a rigid frame is still required to fix the shape of the DEA. For these reasons, there are limitations in implementing DEAs as portable small-scale robots.

For much more complex actuation, DEAs consisting of multiple segments have been developed previously as follows. For examples, Poole et al [27] reported a crawling actuator using multi-stack dielectric elastomers consisted of a silicone dielectric elastomer. Although they introduced multiple folded stacks to generate traveling-wave by sequential actuation of their segments, the maximum locomotion velocity of 2.1 mm/min was obtained that is insufficient values in commercial terms. It means that folded stacks cannot produce relatively large voltage-induced deformations. Jung et al [28] presented a multi-segment robot by employing DEAs inserted in a rigid frame and provided three degree of freedom (3-DoF) motion. These earthworm robots provided stable motions with maximum velocity of 2.5 mm/s. However, it showed the limitation of flexible motion compared to the stack design. In addition, Henke et al [29] developed fully soft skin-like structures robot that can perform locomotion and transportation. They can perform different operation by changing electrodes configuration and voltage application strategies, but each active area produces relatively small deformations.

In the present study, a new design and fabrication process for a multi-balloon actuator is introduced to generate traveling wave motion while maintaining a flexible body. We developed a multi-balloon actuator, which is independently driven by electrical signals and made of soft materials, and developed a control logic for the linear transportation of an object. The remainder of this paper is structured as follows. First, the basic operating mechanism of the balloon actuator is addressed. Next, the design concept and the fabrication method of the multi-balloon actuator are presented. Finally, we present the details of the experimental apparatus and the evaluation results regarding the deformation behavior and the traveling wave motion of the 3–balloon actuator.

2. Design and fabrication of multi-balloon actuators

2.1. Balloon-like Design

The basic characteristics of the perpendicular and planar stains of a non-stretched DEA are described below. The actuation principle of DEAs is illustrated in Fig. 1. When a high voltage is applied to the electrodes, the Maxwell stress that is generated compresses the membrane in the transverse direction, thus expanding in the planar direction. For a linearly elastic membrane, the transverse strain is expressed as follows:

$$\varepsilon_z = \frac{e_r e_0 E^2}{Y} \quad (1)$$

where ε_z is the transverse strain, e_r is the relative permittivity of the polymer, e_0 is the permittivity of free space, E is the applied electric field strength, and Y is the Young's modulus. Most elastomers are incompressible, and the planar strain $\varepsilon_X (= \varepsilon_Y)$ can be written as follows:

$$\varepsilon_X = \frac{1}{\sqrt{1+\varepsilon_z}} - 1 \quad (2)$$

where ε_X and ε_Y represent the planar strains of the horizontal components. The strain curve simulated analytically along the thickness and planar directions is shown in Fig. 2. The specifications of the silicone elastomer (ELASTOSIL® FILM 2030, WACKER) are listed in Table 1. Considering the membrane with an electrode area of 18×18 mm^2 and thickness of 200 μm, the expansion area and thickness reduction obtained by the analytical method are 13.1 mm^2 and 8 μm, respectively. It is noted that the displacement along the thickness direction is too small to be utilized.

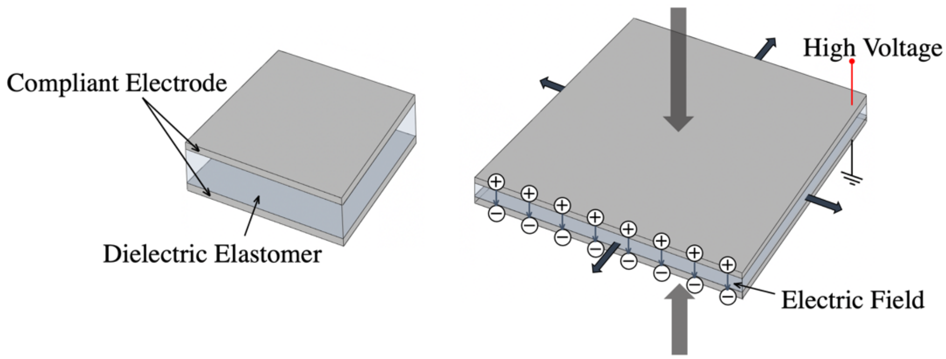

Fig. 1. Structure and actuation principle of a DEA

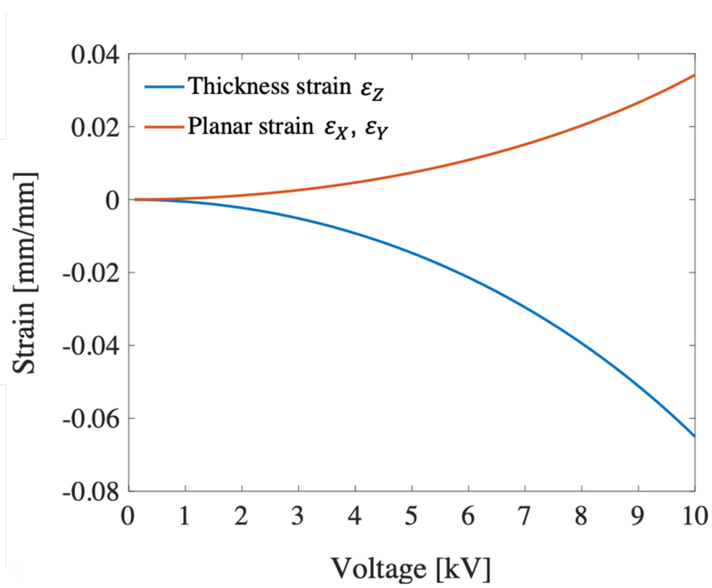

Fig. 2. Strain curve simulated along the thickness and planar directions

Table 1. Specifications of the silicone membrane

Variable	Value
Elastic modulus (MPa)	1.09
Initial thickness (μm)	200
Relative permittivity	2.8

In the present study, the concept of a balloon-like inflated actuator was introduced to obtain large motions in the height and width directions, as shown in Fig. 3. When activated, the balloon immediately inflates due to the expansion of the area of the membrane, thus increasing its height and width. In addition, the membrane that has been pre-expanded with air pressure significantly increases the size of a voltage-triggered deformation. Because the pre-stretch percentage of the membrane is determined by the air pressure, motions in the width and height directions can be controlled prior to actuation.

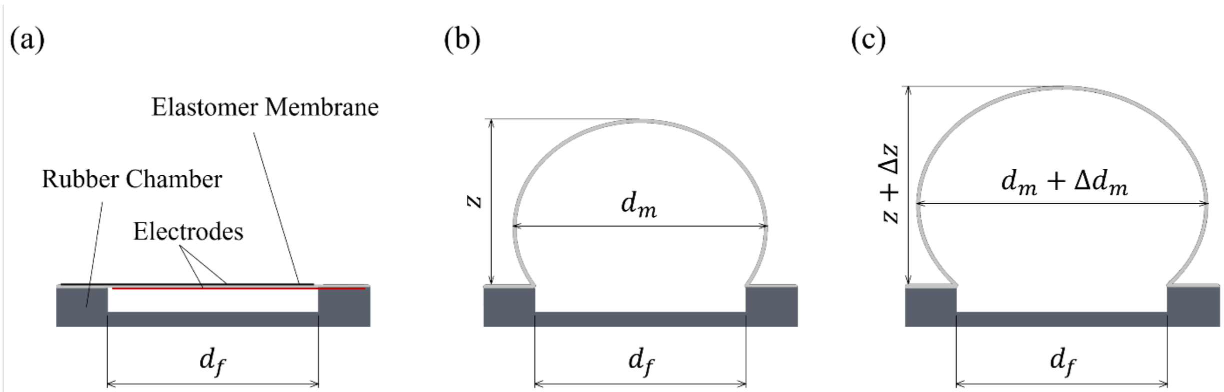

Fig. 3. Schematic view of 1−balloon actuator: (a) Initial state; (b) Pressurized state; and (c) Activated state

Fig. 3 depicts the initial state, pressurized state, and activated state of the 1–balloon actuator. After coating the electrode on the square-shaped membrane, it was mounted in the chamber, as shown in Fig. 3(a). When air pressure is applied, the elastomeric membrane forms a balloon. The expansion is accompanied by thinning of the membrane, as shown in Fig. 3(b). The volume of air enclosed inside the balloon and the chamber is fixed when the valve is closed. Subsequently, a voltage is applied to the membrane thickness to induce further expansion, as shown in Fig. 3(c). To implement a traveling wave in a multi-balloon actuator, an interference between adjacent balloons is required. Therefore, the width d_m must be greater than the gap between each segment d_f for the pressurized state.

2.2 Traveling wave actuator

The proposed multi-balloon actuator with at least two balloons was designed to create the traveling wave motion, as shown in Fig. 4. It mainly consists of an electrode-patterned elastomer membrane and an air chamber. The elastomer membrane is coated with electrodes and acts as an actuator to provide a high response rate, flexible movement, and reliability. It should be noted that each electrode segment is spaced at even intervals and forms an independently controllable balloon. The air chamber can be used to create a flexible body frame and enable each segment to inflate with identical air pressures. In addition, the rubber chamber is sufficient to sustain the tensile force caused by the deformation of the elastomer membrane. The air hose is connected to the air chamber to apply the initial air pressure to the membrane and is then disconnected prior to actuation. The configurations or sizes of the actuators can be changed depending on the shape of the chamber and the electrode patterns, as desired.

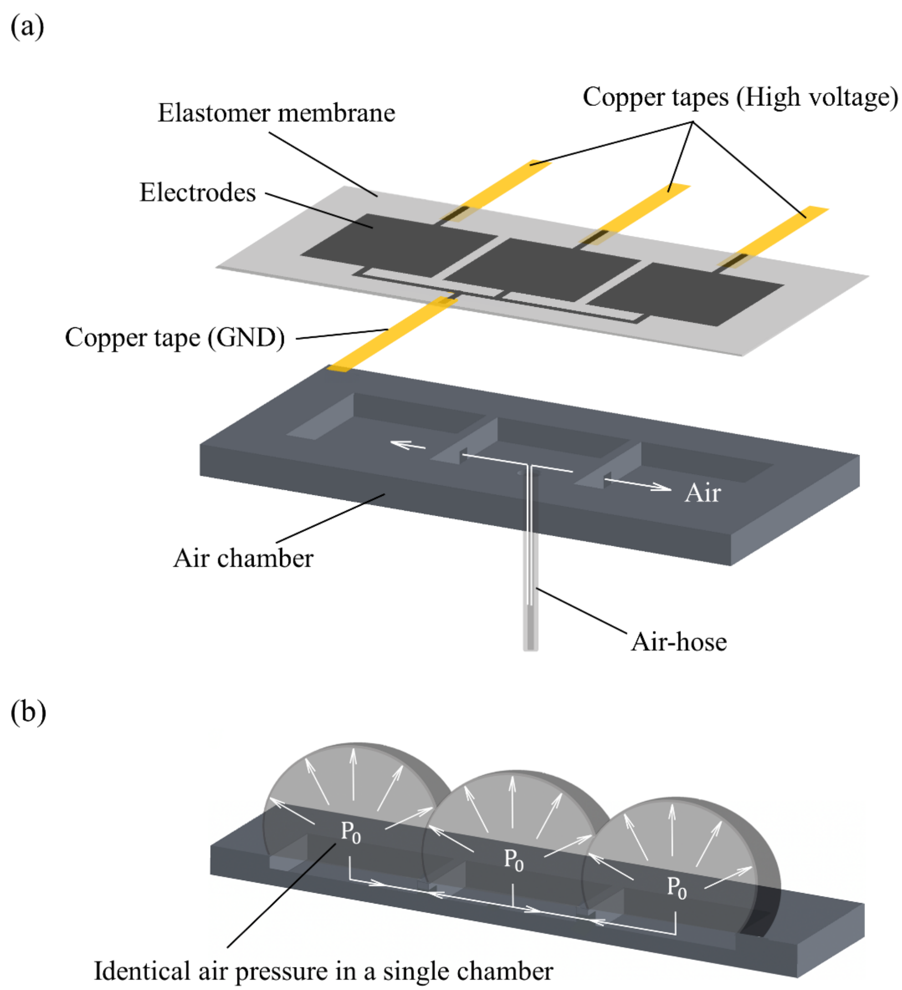

Fig. 4. Schematic diagram of the designed 3–balloon actuator: (a) Actuator parts; and (b) Cross section during a pressurized state

After the pressurized elastomer membrane was stretched from the balloon surface, each balloon was sequentially activated by voltage. The activated balloon provides displacements in the height and width directions so that the interference between adjacent balloons achieves a traveling wave motion. The transportation behavior of the 3–balloon actuator is shown in Fig. 5. The continuous deformation of the activated balloons by voltage application induces a driving force, which enables an object to transport linearly, as shown in Fig. 5(a). Because the air pressure and the center position of the balloon are deformed in real time due to the shape change of the balloons, it is necessary to know the deformation characteristics.

The control system that applies a delicate voltage signal to each balloon segment is shown in Fig. 5(b). To be activated, the elastomer membrane of the 3-balloon actuator has different electrode pattern on both sides. The outer electrode is connected to the ground, whereas the inner electrodes are independently connected to the single-pole double-throw relays via a high voltage generator. The output characteristics of the 3–balloon actuator depend on the driving voltage signal from the microcomputer, which utilizes three power relays (K81C245, TE Connectivity Aerospace) to switch the state of the applied voltage and the short circuit state. If the relay is deactivated, both electrodes of the segment are connected to the ground. As a result, the segment membrane is discharged, and the balloon is deactivated. Besides, when two balloons are activated at the same time, the part they are in contact with is always equal to the ground so that they could keep insulated. The peristaltic wave signal that is applied to each segment is shown in Fig. 5(c).

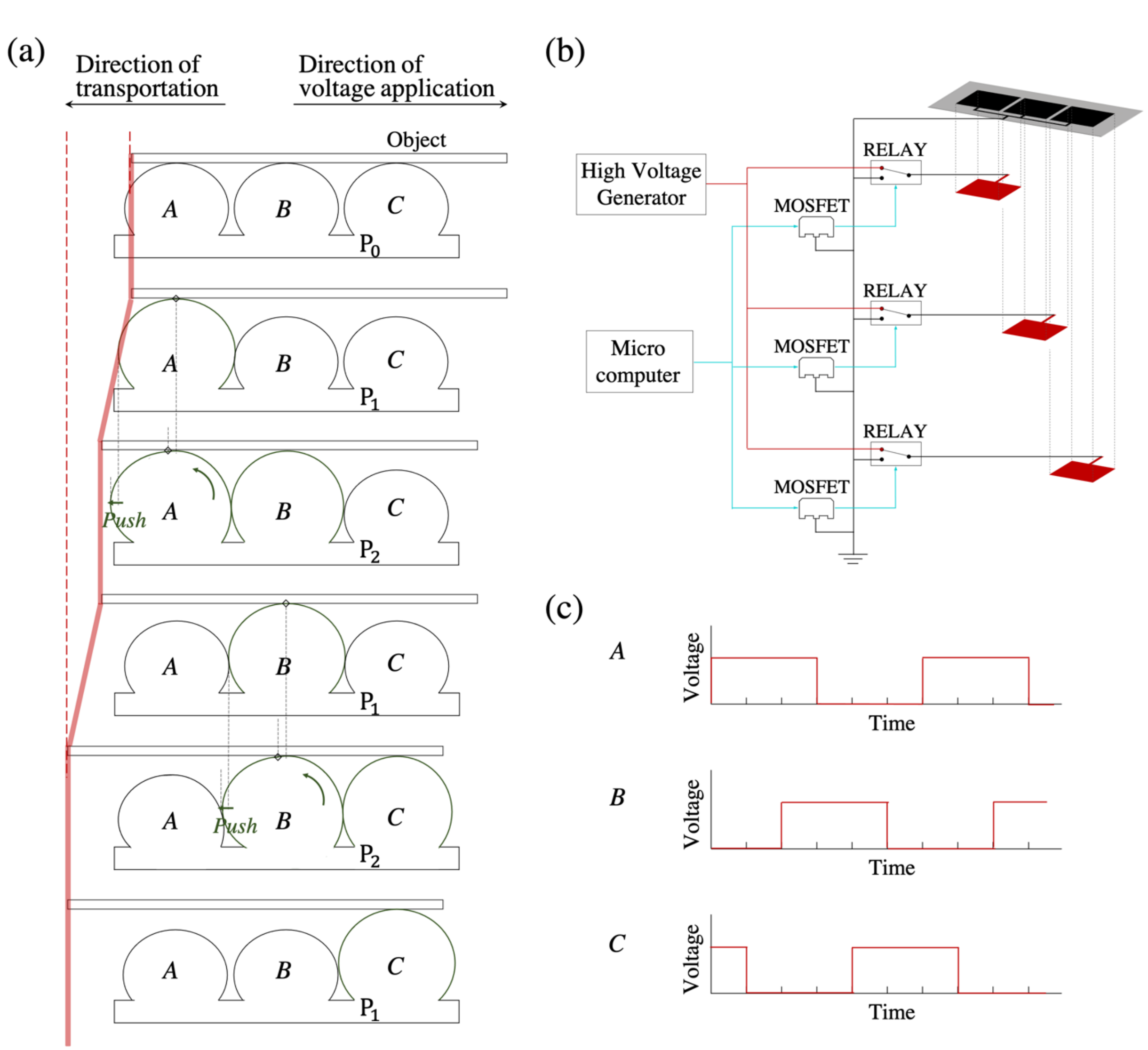

Fig. 5. Transportation behavior of the 3–balloon actuator: (a) Transportation process; (b) Electric circuit for the control system; and (c) Peristaltic wave signal applied to each segment

2.3. Material properties

As mentioned above, the proposed actuator induced by DEA requires large strains, a low modulus, and a high response rate. Considering strains based on the Voigt model and the stress-derived Maxwell model [20], a polymer with a low viscosity and high Young's modulus is desirable. In addition, the stress softening and aging effects of the polymer should be considered to continuously maintain repetitive actuation.

In the present study, a silicone elastomer membrane (ELASTOSIL® FILM 2030, WACKER) was selected considering the response time and stable motion. Because silicone elastomers have a relatively low viscoelasticity compared to acrylic and polyurethane materials, they can be operated at a higher frequency. Silicone elastomer shows little tendency for stress softening and aging effects, resulting in a stable repeatable operation without failure. Although strain-softening elastomers such as acrylic materials tend to decrease in Young's modulus notably after pre-stretching, the silicone elastomer does not show the same strong tendency [30].

In addition, a compliant electrode must be strongly attached to the silicone elastomer and printed with a low thickness. When the thickness of the elastomer membrane and the electrode layer are equal, the composite rigidity increases, which limits the drive deformation of the actuator. A silicone-based carbon paste (ELASTOSIL® LR 3162 A/B, WACKER) was selected in the present study.

2.4. Fabrication

A series of processes are presented to construct the entire soft actuator, as shown in Fig. 6(a). The fabrication process of the 3–balloon actuator is divided into three major steps: 1) Screen-printing of DEAs; 2) Mold casting of the air chamber; and 3) Plasma treatment for bonding. The specific production process is as follows:

1) Screen-printing of DEAs
   - i) Mix the two-component electrode grease and isooctane in a ratio of 1:1:1.25 to adjust the viscosity
   - ii) Place the electrodes on a dielectric elastomer membrane using a screen-printing device
   - iii) Dry at 50 ℃ and evaporate the solvent completely
   - iv) Repeat ii) and iii) on the other side of the membrane

2) Mold casting of an air chamber
   - i) Mix the two-component silicone rubber in specified proportions
   - ii) Pour the mixture into a mold that is the size of an air chamber using a 3D printer
   - iii) Remove the hardened air chamber from the mold

3) Plasma treatment for bonding
   - i) Bond the electrode-printed membrane to the air chamber with plasma processing equipment
   - ii) Make electrical connection with copper tapes and seal the actuator

The electrode-coated elastomer membrane, the molded air chamber, and the fabricated prototype actuator are shown in Fig. 6(b).

As mentioned earlier, most traditional DEAs operate with pre-stretching that is initially provided as a manual process, which can introduce a significant uncertainty in their performance and stability. However, the proposed method can improve the stability of the DEA dynamics because the uncertainty caused by the pre-stretching process is resolved by concrete adhesion prior to inflation. Therefore, the proposed fabrication method has the advantages of eliminating unnecessarily strong parts, improving the stability of the actuator dynamics, and enhancing the adaptability to a variety of actuator configurations.

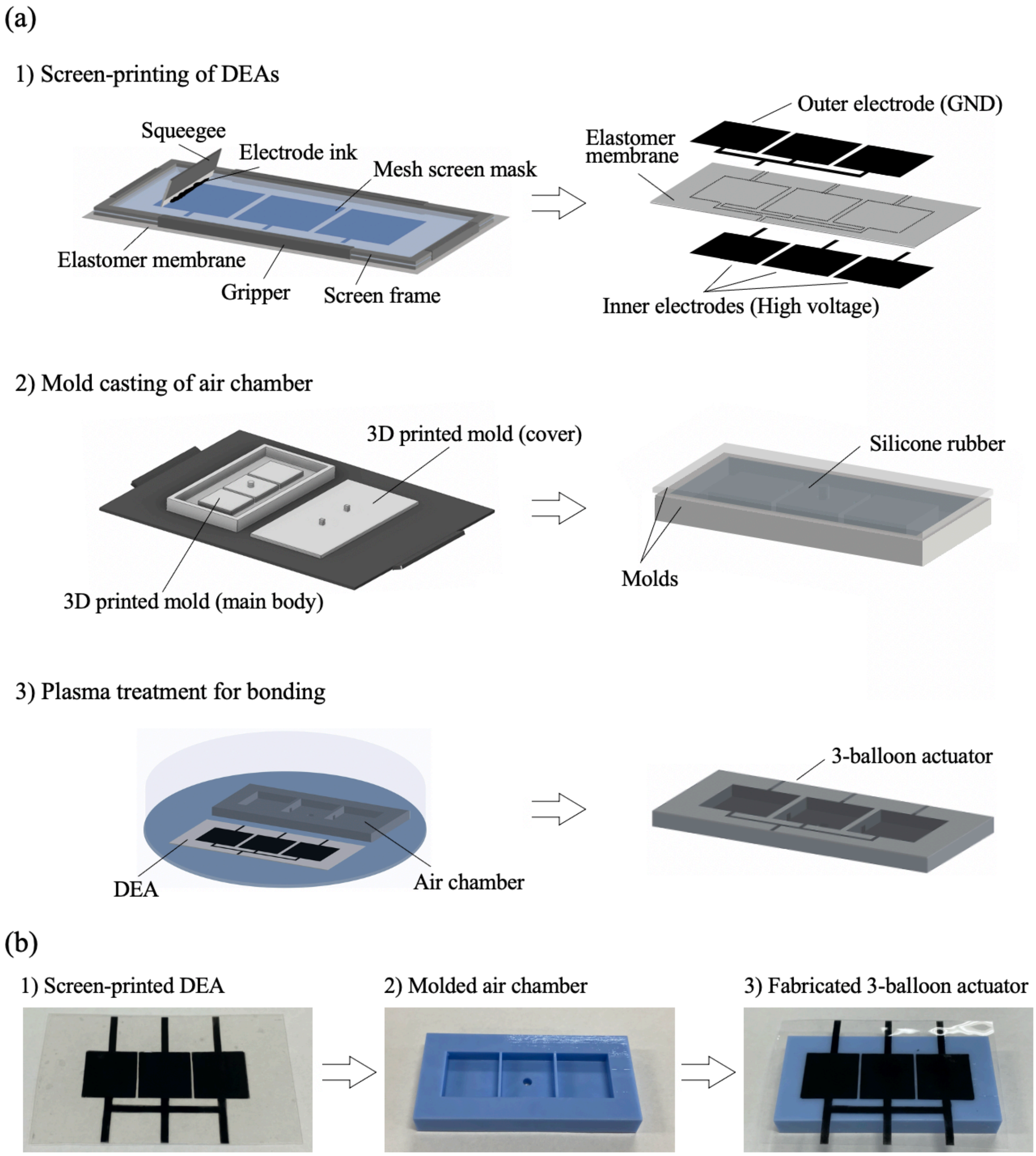

Fig. 6. Fabrication process of a 3–balloon actuator: (a) Schematic diagram of manufacture flow; and (b) Snapshots of a screen-printed DEA, molded air chamber, and fabricated 3–balloon actuator

3. Experiments and discussions

3.1. Experimental apparatus and method

3.1.1. Deformation characteristics

The experimental apparatus for the multi-balloon actuator is shown in Fig. 7. After supplying air pressure to expand it into a multi-balloon structure, the amount of air was fixed when closing the valve. The voltage signal generated by the microcomputer was amplified using a high-voltage power supply (HEOP-10B2, Matsusada Precision Inc.). The deformation of the balloons was tracked and recorded using a video camera and a laser displacement sensor, respectively. In addition, the air pressure in the chamber was measured using a pressure sensor and recorded on an oscilloscope.

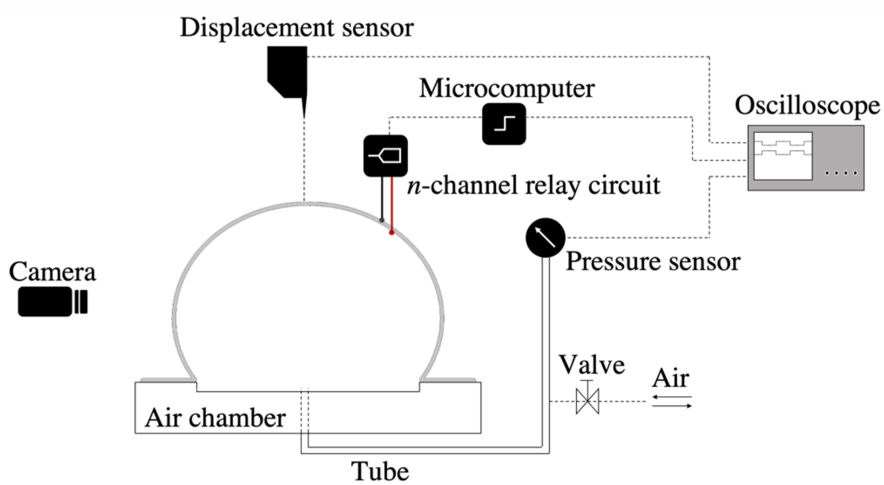

Fig. 7. Experimental apparatus for *n*–balloon actuator

3.1.2 Actuation force

Another experiment of actuation force was performed for the balloon actuator as shown in Fig. 8. To evaluate the achievable force between its surface and the object to be linearly transported, the *X*-axis force on the top of the balloon surface was measured after being activated several times. An obstacle was introduced to implement the movement when the balloon collides with an adjacent balloon after the voltage application. A T-shape cylinder indenter connected with a loadcell (Nano 17, ATI Industrial Automation) was attached to perform little indentation so that the generated force in the *X*-axis direction can be measured without slipping. The force data were recorded using a data acquisition device (NI USB-6343, National Instrument). The internal air pressure and applied voltage were recorded using the measurement devices mentioned above.

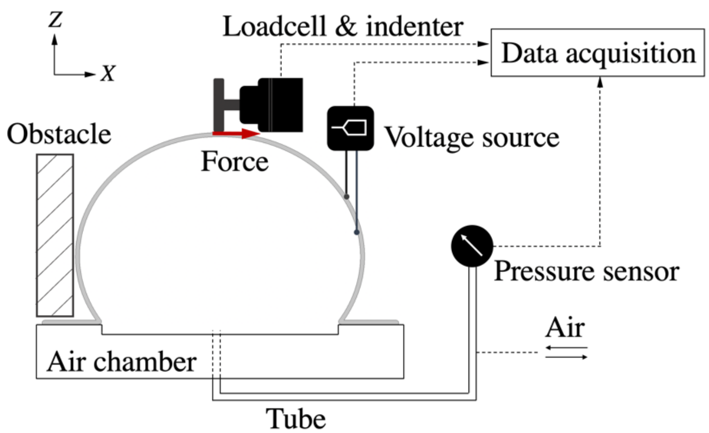

Fig. 8. Force measurement setup for the balloon actuator

3.2. Deformation characteristics of 1–balloon actuator

To evaluate the driving performance of the 1–balloon actuator introduced in this study, we conducted several experiments. The specifications of the multi-balloon actuator, such as the size of the gap between each segment and the thickness of the elastomer membrane, were determined using the obtained results. In addition, to avoid premature failure, a high dielectric breakdown strength was required. Because the actuator depends strongly on the thickness of the elastomer membrane, DEAs with three different thicknesses (50, 100, and 200 μm) were fabricated and tested.

Although the width of each balloon actuator must be inflated so that there is sufficient interference between adjacent segments, the actuators used in this study with thicknesses of 50 and 100 μm experienced dielectric breakdown prior to meeting this condition. As a result, we demonstrate that DEAs with thicker membranes can produce sufficient strains to obtain traveling waves in the proposed design concept. Therefore, DEAs with a thickness of 200 μm were selected for the present experiments.

The measurement was performed with the following three items: 1) A change in shape before and after electrical operation; 2) A height displacement with respect to initial pressure; and 3) An increase in the width relative to the initial width. The results for the volume differences of the electric stimulus of the balloon actuator under an air pressure of 12.2 kPa are provided in Figs. 9 and 10. Note that the shape of the inflated balloon was transformed into an ellipse, and the position of the center moved along the Z-axis during actuation.

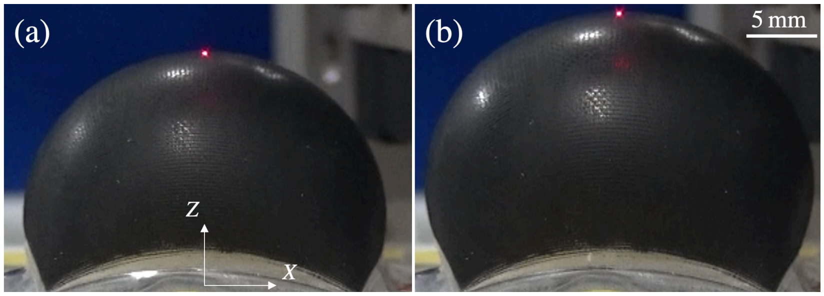

Fig. 9. Photograph of the 1–balloon actuator at the initial pressure of 12.2 kPa: (a) 0 kV; and (b) 9 kV

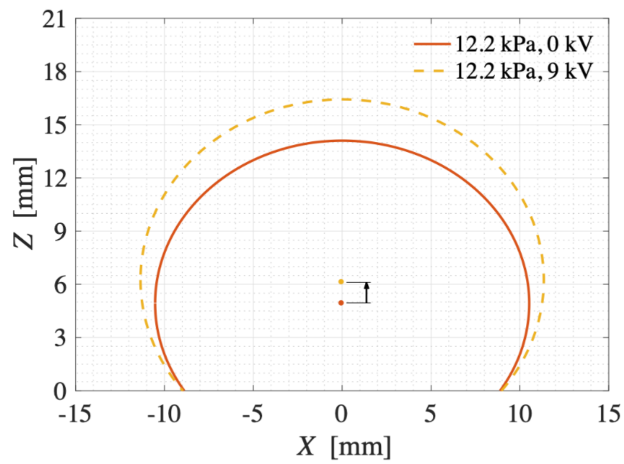

Fig. 10. Comparisons of the balloon actuator at the initial pressure of 12.2 kPa (black arrow indicates the change in the center of the ellipses)

The motion characteristics of pre-stretching, controlled by the initial pressure, were evaluated. The height displacements of the balloon actuator measured at the applied voltages of 8 kV and 9 kV are shown in Fig. 11. The height displacement gradually decreased after peaking near the initial pressure of 12.2 kPa. The maximum height displacements obtained were 1.57 mm and 2.28 mm for the applied voltage of 8 kV and 9 kV, respectively.

Fig. 12 shows the change in the width of the balloon actuator with respect to the initial pressure for different voltages. For the inflated balloon actuator with an initial width of 21.1 mm, a width change of 1.64 mm was obtained when the applied voltage was 9 kV. For the pressurized balloon with an initial width of 22.3 mm, the width change was 1.05 mm under the condition of a voltage of 8 kV. This confirms that the width deformation has the maximum value within the initial pressure of 12.2 kPa. Although the area strain of the balloon surface increased by pre-stretching, these results indicate that the relationship between displacement and pressure is non-linear.

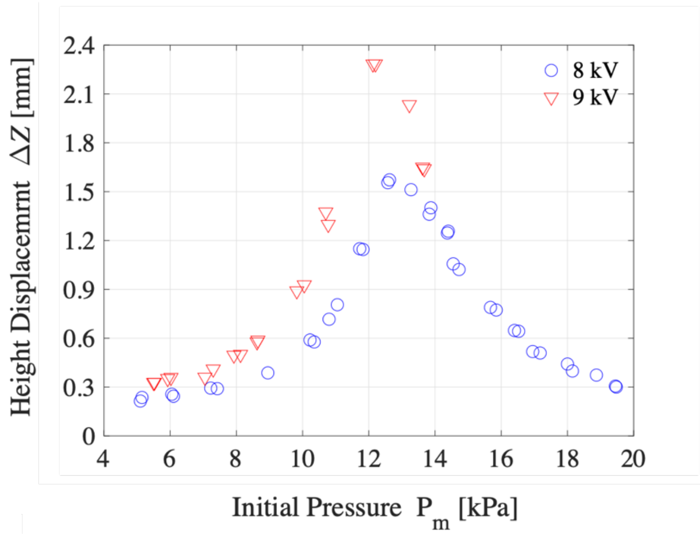

Fig. 11. Height displacement of the balloon actuator with respect to initial pressure for 8 kV and 9 kV

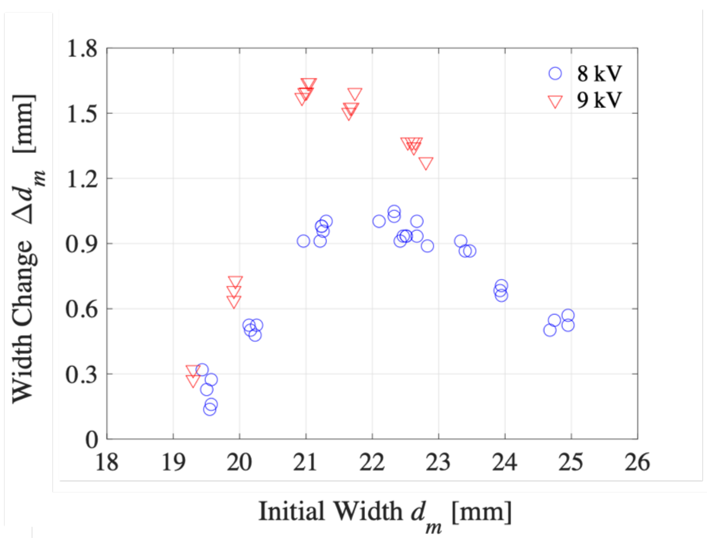

Fig. 12. Width change of the balloon actuator with respect to initial width for 8 kV and 9 kV

3.3. Actuation force of 1–balloon actuator

The actuation force test was performed for the balloon actuator of the inflated state to an air pressure of 13.2 kPa. Specifically, at the pressurized state, the obstacle and indenter were located on the side and top of the balloon, respectively. After activated, the balloon expanded further and was pushed by the obstacle, compressing the indenter so that force was measured. Fig. 13 shows the recorded force when the balloon was actuated with different voltages. As shown in the figure, the *X*-axis force linearly increases as voltage increases. It is noted that the maximum force in the *X*-axis direction has about 550 mN.

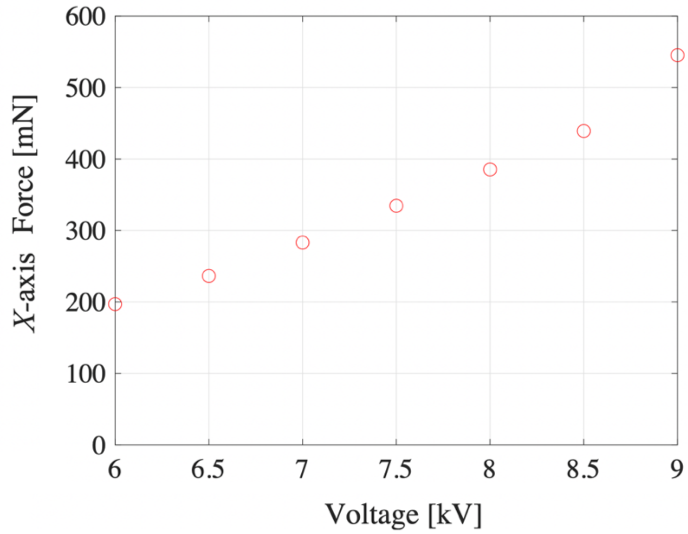

Fig. 13. *X*-axis force of the balloon actuator with respect to voltage at the pressure of 13.2 kPa

3.4. Motion tracking of 3– balloon actuator

In the present study, a 3–balloon actuator with an interval of 1 mm between the balloons was developed. The electromechanical actuation of the individual segment induced the three balloons to interfere with each other to obtain a traveling wave motion. In addition, each balloon was able to produce a frictional force between its surface and the object, thus transporting an object linearly. The deformation induced by the force between the activated balloons was evaluated. The possibility of generating a traveling wave in the desired direction was observed by a continuous measurement using a two-way voltage application. The obtained deformations in a working process of the 3–balloon actuator under an applied voltage of 7.5 kV and air pressure of 14.6 kPa are provided in Fig. 14.

Fig. 15 shows the locations of the markers, the voltage waves applied to the three segments, and the tracking results for an applied voltage of 7.5 kV and air pressure of 13.2 kPa. As shown in the figure, each marker is plotted on the top of the balloons, and its position is captured in the photograph, while a voltage signal was applied in either the forward (A→B→C) or backward (C→B→A) direction. Each state is indicated in response to an applied voltage signal from an inactive state (indicated by 0) to an active state (indicated by 1-5).

When a sequential electrical stimulus is applied along the forward direction, as shown in Fig. 15(a), markers A and B are pushed in the negative X-direction by the activation, thus causing the contacted object to advance backward. For interfering segments, such as the markers in A (states 1-2) and markers in B (states 3-4), movement in the down-left direction is observed. Alternatively, segment *C* of the 3–balloon actuator cannot contribute to the transport of the object as there are no successive segments that are active and capable of interacting further. Furthermore, a small movement along the negative Z-direction that is induced by pressure drops with internal volume increases was observed for markers A and B. However, these changes were negligible compared to the voltage-induced displacement, and the interaction between the balloons was sufficient.

When voltage is applied in the backward direction, as shown in Fig. 15(b), the movement of markers B and C indicates that the top of the balloon is positively pushed in the X-direction by the activation. Taken together, these experimental results demonstrate the effectiveness of the designed transportation principle using the 3–balloon actuator.

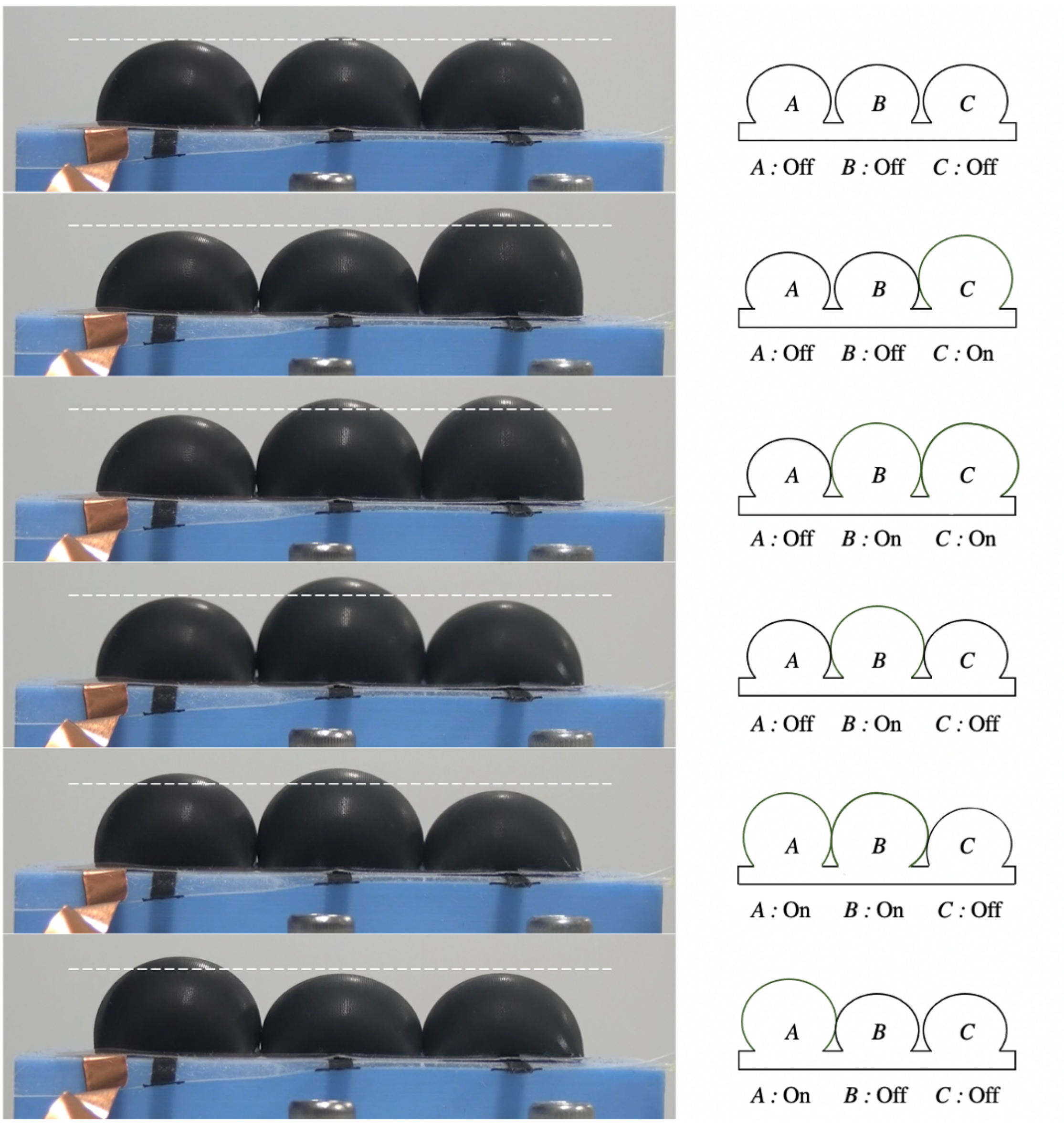

Fig. 14. Snapshot of the 3–balloon actuator deformation with an applied voltage of 7.5 kV and pressure of 14.6 kPa

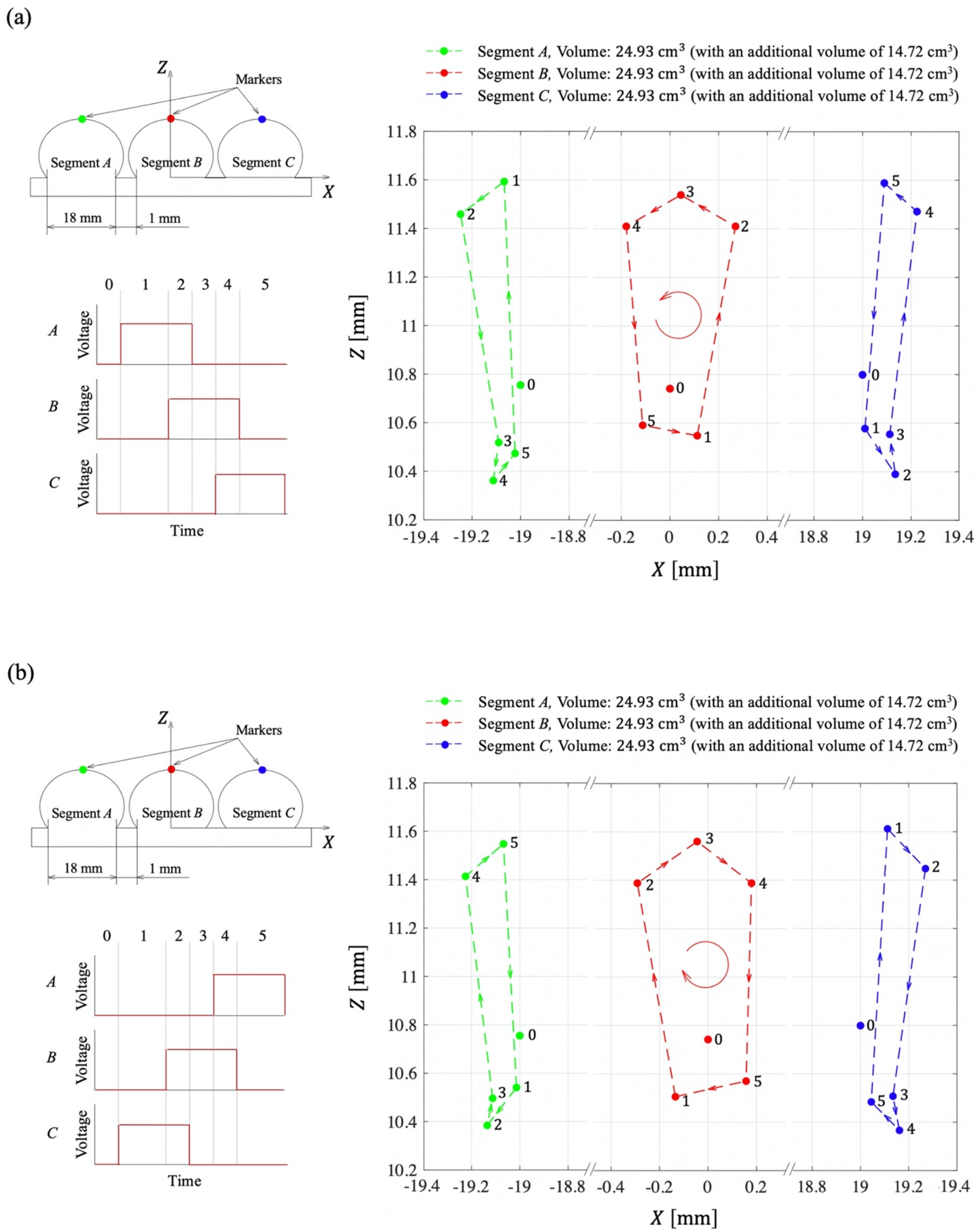

Fig. 15. Marker position on each segment and tracking results with an applied voltage of 7.5 kV and pressure of 13.2 kPa: (a) Forward voltage signal; and (b) Backward voltage signal

In the previous experiments, the air hose and air supplier were connected to control the initial air pressure. With the larger internal space of the actuator, including the mechanical elements, the pressure drop could be suppressed as the voltage-induced volume increased during operation. To prove the possibility of a portable multi-balloon actuator without an air hose, an experiment using a 3–balloon actuator was conducted. Tracking tests were performed after setting the pressurized actuator to an internal pressure of 13.2 kPa, without additional volumetric elements. Fig. 16 shows the behavior of the pressure and the marker position with different volumes under an applied voltage of 7.5 kV and a pressure of 13.2 kPa. The internal volumes in the previous and present experiments were 24.93 cm^3 and 10.21 cm^3, respectively. We found that the air hose-free actuator was also capable of performing repeated traveling wave motions. The pressure over time and the marker tracking showed little difference when compared at different volumes. The pressure changes associated with voltage-induced deformation did not have a significant effect on traveling wave generation without the additional devices. Therefore, the developed actuator can perform well in portable applications.

(a)

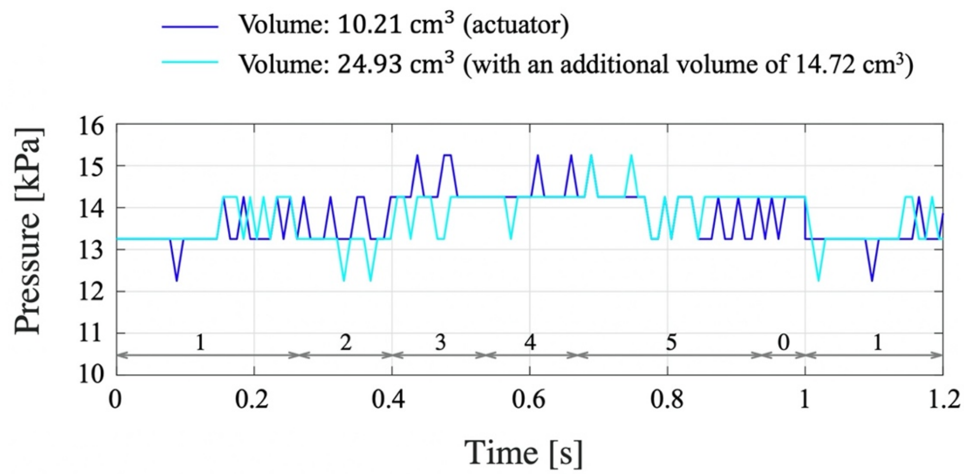
Volume: 10.21 cm³ (actuator)
Volume: 24.93 cm³ (with an additional volume of 14.72 cm³)
Pressure [kPa]
Time [s]
16
15
14
13
12
11
10
0
0.2
0.4
0.6
0.8
1
1.2
1
2
3
4
5
0
1

(b)

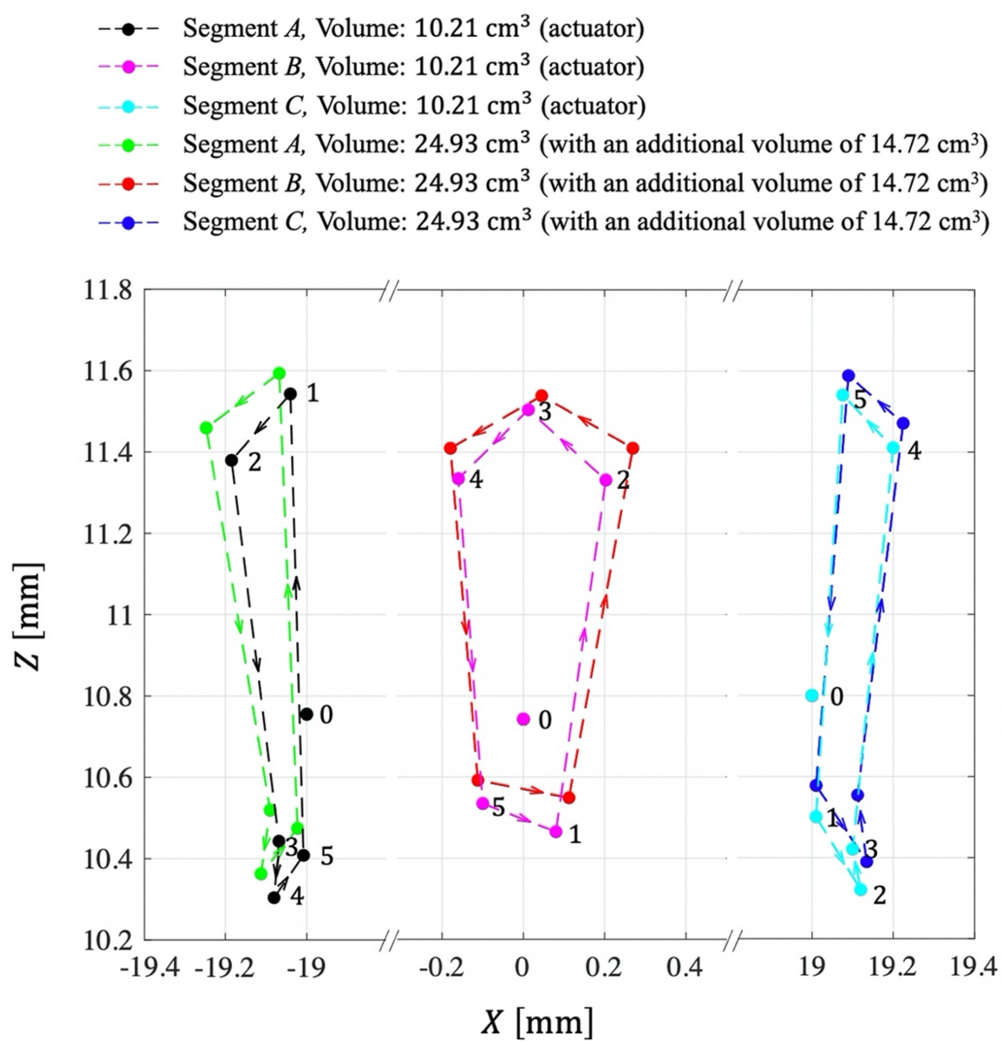
Segment A, Volume: 10.21 cm³ (actuator)
Segment B, Volume: 10.21 cm³ (actuator)
Segment C, Volume: 10.21 cm³ (actuator)
Segment A, Volume: 24.93 cm³ (with an additional volume of 14.72 cm³)
Segment B, Volume: 24.93 cm³ (with an additional volume of 14.72 cm³)
Segment C, Volume: 24.93 cm³ (with an additional volume of 14.72 cm³)
Z [mm]
X [mm]
11.8
11.6
11.4
11.2
11
10.8
10.6
10.4
10.2
-19.4
-19.2
-19
-0.2
0
0.2
0.4
19
19.2
19.4

Fig. 16. Behavior of pressure and the marker position with different volumes under an applied voltage of 7.5 kV and a pressure of 13.2 kPa: (a) Internal pressure over time; and (b) Marker position tracking

3.4. Transportation of 3–balloon actuator

The main test for the 3–balloon actuator was the evaluation of its ability to perform linear transportation and the velocity of that transportation. To verify the ability of the 3–balloon actuator to perform linear transportation, a paper target was employed as an object. Although it was not possible to determine the exact pressure value that achieved the maximum strain, in this experiment, the initial pressure was set at 13.3 kPa so that the balloons could sufficiently interact with each other. The transportation test was recorded with a video camera. Fig. 17 shows snapshots of the paper transportation tests when each balloon was activated sequentially in the forward and backward directions. These results demonstrate that the paper was successfully moved in the desired direction. The maximum velocity was 0.97 mm/s at an applied voltage of 7.5 kV, 1 Hz.

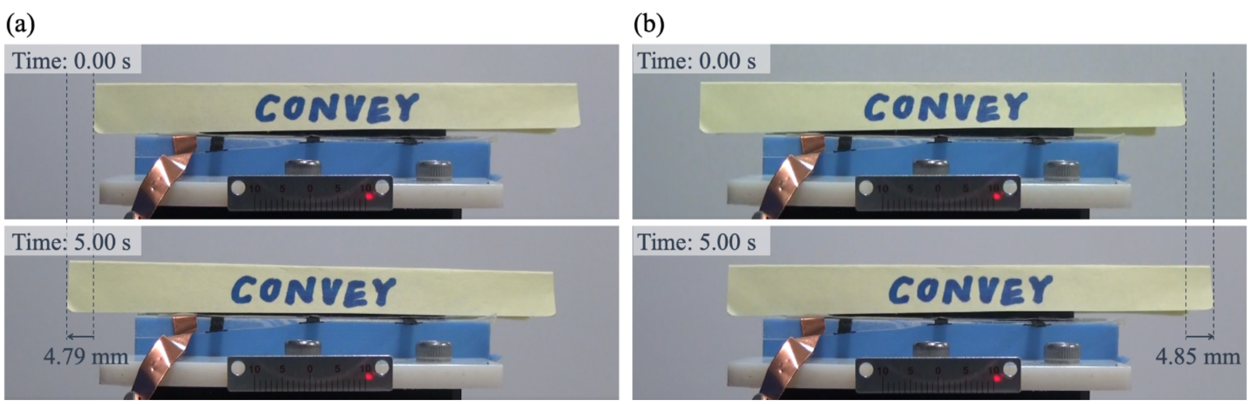

Fig. 17. Snapshots of the paper transported by the 3–balloon actuator with a pressure of 13.3 kPa and a voltage of 7.5 kV, 1 Hz: (a) Forward voltage signal; and (b) Backward voltage signal

Fig. 18 shows the resulting linear velocity exhibited by the 3–balloon actuator, given different air pressures. The falling curve indicates a good correspondence in the descending curves of the displacement–pressure for the 1–balloon actuator. Although the peak of the curve was not obtained in the present test, the pressure of 13.3 kPa seems to slightly exceed the optimum pressure from the previous experimental results. That is, to achieve higher rates of speed, it is essential to obtain high strain rates. In addition, the recorded velocities in the two actuated cycles were qualitatively consistent.

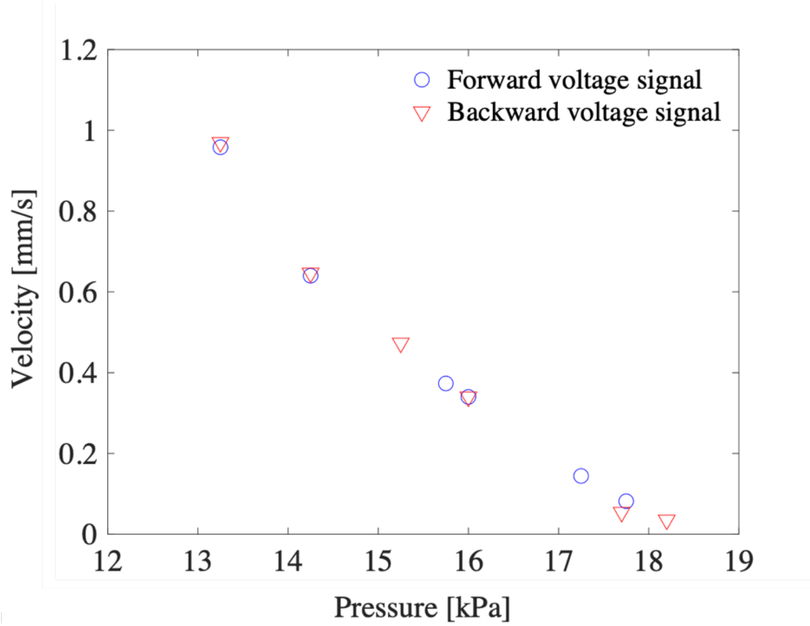

Fig. 18. Transportation velocity for 3–balloon actuator at a voltage of 7.5 kV, 1 Hz

4. Conclusion

A novel multi-balloon actuator based on a silicone elastomer was developed to generate a traveling wave motion for the linear transportation of an object. By designing a 3–balloon actuator with flexible and reproducible motion, a control method for the linear transportation of objects is introduced. The actuator consists of an electrode-patterned polymer combined with an elastic body that replaces the conventional rigid frame using the proposed fabrication process. Several experiments were performed to verify the performance of the developed actuator. The results are summarized as follows:

The maximum deformation of the balloon was obtained in a specific pressure range of 12.2 kPa. When we used a piece of paper as a moving object, a transportation velocity of 0.97 mm/s was obtained using an initial air pressure and an applied voltage of 13.3 kPa and 7.5 kV, respectively. The present air-hose-free actuator generated a traveling wave motion with little difference from the version with a hose, although the internal space configuration was changed by removing the air supply equipment while operating at the same air pressure. From the tracked motions of a multi-balloon actuator, the effectiveness of the novel actuation method was demonstrated, with the possibility of its application as a portable robot. The proposed fabrication method shows the possibility of constructing a variety of soft actuators with microscale size, that are lightweight, and have stable dynamics.

This actuator still has room for improvement in terms of actuation frequency, which is currently fixed at 1 Hz. Due to the rapid response speed of DEAs, the actuator can produce much faster transportation by increasing the frequency. It may be achieved by additional experiments to demonstrate the displacement-frequency curve and determine the maximum value. In addition, a theoretical model will be addressed, thus enables a variety of configurations for balloon DEAs with desired shapes.

Improvements regarding the energy density are still required for the real robot implementation. Compared to the inflated elastomer membrane that functions as actuator, the mass (or volume) of the rubber become non-negligible when considering the energy density. However, in the present stage, the rubber is essential to from the balloon structure and the optimum study to maximize energy density does not performed. These issues will be challenging tasks for the further development of the traveling wave actuator as the future works.

Authors' statement

Yujin Jang: Investigation, Methodology, Visualization, Writing – original draft
Hiroyuki Nabae: Supervision, Writing – review & editing
Gen Endo: Supervision
Koichi Suzumori: Conceptualization, Supervision, Writing – review & editing

Declaration of Competing Interest

The authors report no declarations of interest.

Acknowledgement

This work was supported by JSPS KAKENHI under Grant 18H05470.

References

[1] J. H. Goldie, M. J. Gerver, J. E. Kiley, J. R. Swenbeck, Observations and theory of Terfenol-D inchworm motors, Smart Struct. Mater. 3329 (1998). https://doi.org/10.1117/12.316948.

[2] X. Qi, H. Shi, T. Pinto, X. Tan, A Novel Pneumatic Soft Snake Robot Using Traveling-Wave Locomotion in Constrained Environments, IEEE Robot. Autom. Lett. 5 (2020) 1610-1617. https://doi.org/10.1109/LRA.2020.2969923.

[3] A. Suleman, S. Burns, D. Waechter, Design and modeling of an electrostrictive inchworm actuator, Mechatronics 14 (2004) 567-586. https://doi.org/10.1016/j.mechatronics.2003.10.007.

[4] L. Xu, H. Q. Chen, J. Zou, W. T. Dong, G. Y. Gu, L. M. Zhu, X. Y. Zhu, Bio-inspired annelid robot: a dielectric elastomer actuated soft robot, Bioinspir. Biomim. 12 (2017). https://doi.org/10.1088/1748-3190/aa50a5.

[5] R. Kornbluh, R. Pelrine, J. Eckerle, J. Joseph, Electrostrictive polymer artificial muscle actuators, Proc. 1998 IEEE International Conference on Robotics and Automation 3 (1998). https://doi.org/10.1109/ROBOT.1998.680638.

[6] K. Suzumori, S. Endo, T. Kanda, N. Kato, H. Suzuki, A Bending Pneumatic Rubber Actuator Realizing Soft-bodied Manta Swimming Robot, IEEE International Conference on Robotics and Automation (2007). https://doi.org/10.1109/ROBOT.2007.364246.

[7] K. Suzumori, T. Maeda, H. Wantabe, T. Hisada, Fiberless flexible microactuator designed by finite-element method, IEEE. ASME 2 (1997) 281-286. https://doi.org/10.1109/3516.653052.

[8] S. Wakimoto, K. Suzumori, Fabrication and basic experiments of pneumatic multi-chamber rubber tube actuator for assisting colonoscope insertion, IEEE International Conference on Robotics and Automation (2010). https://doi.org/10.1109/ROBOT.2010.5509633.

[9] T. Noritsugu, D. Kaneshiro, T. Inoue, Soft Planar Actuator using Pneumatic-Rubber Balls, J. Robotics and Mechatronics 12 (2000) 254-260.

[10] R. Pelrine, R. Kornbluh, Q. Pei, J. Joseph, High-Speed Electrically Actuated Elastomers with Strain Greater Than 100%, Sci. 287 (2000) 836-839. https://doi.org/10.1126/science.287.5454.836.

[11] R. Pelrine, R. D. Kornbluh, Q. Pei, S. Stanford, S. Oh, J. Eckerle, R. J. Full, M. A. Rosenthal, K. Meijer, Dielectric elastomer artificial muscle actuators: toward biomimetic motion, Smart Struct. Mater. 4695 (2002). https://doi.org/10.1117/12.475157.

[12] B. O'Brien, E. Calius, S. Xie, I. Anderson, An experimentally validated model of a dielectric elastomer bending actuator, Proc. SPIE 6927 Electroactive Polymer Actuators and Devices (EAPAD) 69270T (2008). https://doi.org/10.1117/12.776098.

[13] F. Carpi, G. Frediani, S. Turco, D. D. Rossi, Bioinspired Tunable Lens with Muscle-Like Electroactive Elastomers, Adv. Funct. Mater. 21 (2011) 4152-4158. https://doi.org/10.1002/adfm.201101253

[14] S. Hau, G. Rizzello, S. Seelecke, A novel dielectric elastomer membrane actuator concept for high-force applications, Extrem. Mech. Lett. 23 (2018) 24-28. https://doi.org/10.1016/j.eml.2018.07.002.

[15] N. Correll, Ç. D. Önal, H. Liang, E. Schoenfeld, D. Rus, Soft Autonomous Materials-Using Active Elasticity and Embedded Distributed Computation, Springer Tracts. Adv. Robot. 79 (2014). https://doi.org/10.1007/978-3-642-28572-1_16.

[16] J. Zhu, S. Cai, Z. Suo, Nonlinear oscillation of a dielectric elastomer balloon, Polym. Int. 59 (2010) 378-383. https://doi.org/10.1002/pi.2767.

[17] S. Ho, H. Banerjee, Y. Y. Foo, H. Godaba, W. M. M. Aye, J. Zhu, C. H. Yap, Experimental characterization of a dielectric elastomer fluid pump and optimizing performance via composite materials, J. Intell. Mater. Syst. Struct. 28 (2017) 3054-3065. https://doi.org/10.1177/1045389X17704921.

[18] R. F. Shepherd, F. Ilievski, W. Choi, S. A. Morin, A. A. Stokes, A. D. Mazzeo, X. Chen, M. Wang, G. M. Whitesides, Multigait soft robot, Proc. Natl. Acad. Sci. USA (2011). https://doi.org/10.1073/pnas.1116564108.

[19] J. Ashby, S. Rosset, E. -F. M. Henke, I. Anderson, Inflatable dielectric elastomer robots for space, Proc. SPIE 10966 Electroactive Polymer Actuators and Devices (EAPAD) XXI 109661L (2019). https://doi.org//10.1117/12.2514227.

[20] Z. Li, J. Zhu, C. C. Foo, C. H. Yap, A robust dual-membrane dielectric elastomer actuator for large volume fluid pumping via snap-through, Appl. Phys. Lett. 111 (2017). https://doi.org/10.1063/1.5005982.

[21] S. Mun, S. Yun, S. Nam, S. K. Park, S. Park, B. J. Park, J. M. Lim, K. U. Kyung, Electro-Active Polymer Based Soft Tactile Interface for Wearable Devices, IEEE Trans. Haptics 11 (2018) 15-21. https://doi.org/10.1109/TOH.2018.2805901.

[22] N. Hosoya, H. Masuda, S. Maeda, Balloon dielectric elastomer actuator speaker, Applied Acoustics 148 (2019) 238-245. https://doi.org/10.1016/j.apacoust.2018.12.032.

[23] F. Wang, C. Yuan, T. Lu, T.J. Wang, Anomalous bulging behaviors of a dielectric elastomer balloon under internal pressure and electric actuation, J. Mech. Phys. Solids 102 (2017). https://doi.org/10.1016/j.jmps.2017.01.021.

[24] T. Li, C. Keplinger, R. Baumgartner, S. Bauer, W. Yang, Z. Suo, Giant voltage-induced deformation in dielectric elastomers near the verge of snap-through instability, J. Mech. Phys. Solids 61 (2013) 611-628. https://doi.org/10.1016/j.jmps.2012.09.006.

[25] C. Keplinger, T. Li, R. Baumgartner, Z. Suo, S. Bauer, Harnessing snap-through instability in soft dielectrics to achieve giant voltage-triggered deformation, Soft Matter 8 (2012) 285-288. https://doi.org/10.1039/C1SM06736B.

[26] H. Godaba, C. C. Foo, Z. Q. Zhang, B. C. Khoo, J. Zhu, Giant voltage-induced deformation of a dielectric elastomer under a constant pressure, Appl. Phys. Lett. 105 (2014). https://doi.org/10.1063/1.4895815.

[27] A. D. Poole, J. D. Booker, C. L. Wishart, N. McNeill, P. H. Mellor, Performance of a Prototype Traveling-Wave Actuator Made from a Dielectric Elastomer, IEEE. ASME 3 (2012) 525-533. https://doi.org/10.1109/TMECH.2011.2107526.

[28] K. Jung, J. C. Koo, J. Nam, Y. K. Lee, H. R. Choi, Artificial annelid robot driven by soft actuators, Bioinspir. Biomim. 2 (2007). https://doi.org/10.1088/1748-3182/2/2/S05.

[29] J. Guo, C. Xiang, A. Conn, J. Rossiter, All-Soft Skin-Like Structures for Robotic Locomotion and Transportation, Soft Robotics 7 (2020). http://doi.org/10.1089/soro.2019.0059.

[30] F. B. Madsen, L. Yu, P. Mazurek, A. L. Skov, A simple method for reducing inevitable dielectric loss in high-permittivity dielectric elastomers, Smart Mater. Struct. 25 (2016). https://doi.org/10.1088/0964-1726/25/7/075018.